Stanford Exploration Project, Report 117, October 23, 2004, pages 27–42

Incorporating topography into wave-equation imaging through conformal mapping

Jeff Shragge and Paul Sava[1]

ABSTRACT

Conformal mapping is a technique used widely in applied physics and engineering fields to facilitate numerical solution of boundary value problems involving solution domains characterized by complex geometry. The predominant reason for applying a conformal mapping procedure is to transform an irregular solution domain to one of symmetric geometry. The conformal map transform has the property that the angle between neighboring arc segments is (locally) conserved under the mapping. Accordingly, in the context of wave-equation imaging under topography, conformal mapping can transform an irregular, topographically-influenced solution domain to a regular computational mesh. In this paper, we demonstrate that the use of the conformal mapping transform coupled with Riemannian wavefield extrapolation generates an orthogonal coordinate system and the governing wavefield contination equation required for wave-equation migration directly from a topographic surface. We illustrate the potential of this approach by migrating a 2-D prestack data set acquired on a geologic model of thrust belt.

INTRODUCTION

Migration of seismic land data acquired on topography presents a significant imaging challenge. One technique used to correct for the deleterious effects of topography in a more accurate fashion than simple statics corrections is to include a wavefield datuming step in the processing flow (Berryhill, 1979). Usually, this step propagates wavefields down to a common subsurface depth level. However, the presence of strong lateral velocity contrast directly beneath the surface can generate significant wavefield triplication that leads to non-optimal datuming results, especially if Kirchhoff-based methods are used. Therefore, a migration workflow that includes an upward or downward wavefield continuation processing step should produce better imaging results.

However, in practice wavefield continuation is seldom applied directly to data sets acquired on topography without significant preprocessing. The predominant challenge is that the metric of source and geophone arrays seldom conform to a regular computational mesh. Rather, due to instrument cabling, geophone arrays are more likely to uniformly sample the topographic surface. Two common solutions to this problem are either to employ a migration

[1]**email:** jeff@sep.stanford.edu,paul@sep.stanford.edu

procedure involving wavefield injection (Jiao et al., 2004), or to perform an upward-datuming prior to migration (Bevc, 1997). Migration by wavefield injection commences at the global topographic maximum where the data recorded at this station are injected into the wavefield. The wavefield is then continued downward and data are injected into the wavefield whenever the extrapolation step reaches the height of the topography. Two drawbacks of this approach are that data need to be regularized beforehand to a uniform grid usually through interpolation, and that the additional number of fine-scale extrapolation steps significantly increase cost. Upward wavefield datuming or "flooding the topography" procedures are employed to generate a regular wavefield above the highest point. This processing step can be done successfully with Kirchhoff or other migration operators. One downside of this approach is, again, the increased preprocessing cost. In general, although these methods produce good results, a significant amount of data preprocessing is required to render Cartesian-based wave-equation migration approaches applicable and, as a result, data fidelity may be compromised.

In this paper, we argue that many of the difficulties with state-of-the-art migration from topography technology could be precluded by abandoning the Cartesian coordinate system for one conformal with the topographic surface. To find such a method, we observe that wave-equation imaging is a specific example of a boundary value problem (BVP) that has a solution domain defined by a polygonal boundary. (Images are the superposition of the monochromatic solutions to a number of BVPs of different frequency.) This observation motivates us to examine the results of other applied fields that routinely solve BVPs, such as aerospace and mechanical engineering.

One method routinely employed to help solve BVPs is conformal mapping. This procedure defines how to transform the physical solution domain to a more symmetric canonical domain through mapping in the complex plane (Kythe, 1998). Relating this concept to wave-equation imaging from topography, we suggest using conformal mapping to transform the topographically-influenced physical domain to a canonical domain characterized by a rectangular computational grid. We term this new orthogonal calculation mesh a "topographic" coordinate system. Moreover, the forward and inverse conformal map transforms are also used in defining the wavefield extrapolation equations appropriate for the canonical domain. Consequently, we are both able to perform wavefield extrapolation and to apply the imaging condition in the topographic coordinate domain. The final image is generated by mapping the topographic coordinate image to the physical domain using the inverse conformal mapping transform.

We begin the paper with an overview of conformal mapping illustrated by some simple examples. We then review Riemannian wavefield extrapolation (Sava and Fomel, 2004) and the steps required to generate appropriate wavefield extrapolation equations. Prestack migration results are presented for a data set acquired over a 2-D geological model characterized by severe elevation relief, strong near-surface velocity contrast, and complicated folding and faulting. The paper concludes with a discussion on the relative merits and drawbacks of the proposed approach.

CONFORMAL MAPPING

Conformal mapping is a topic of wide-spread interest in the field of applied complex analysis. Generally, this subject deals with the manner in which point sets are mapped between two different analytic domains in the complex plane. In this paper, we refer only to domains that are simply- (i.e. not multiply) connected. A mapping between complex planes may be thought of as a rule relating how a field of points defined on a domain in the z-plane, $z = x + iy$, maps to the w-plane, $w = u(x,y) + iv(x,y)$, according to a mapping function, $w = f(z)$ (see the example in Figure 1). If for each point in the z-plane domain there corresponds a unique number in the w-plane, then the mapping function is analytic. In addition, if for each point in the w-plane there corresponds precisely one point in the z-plane, then the mapping is one-to-one and the transformation is invertible. The Cauchy-Riemann equations (Nehari, 1975) are the necessary and sufficient conditions for function $f(z)$ to be analytic in a domain of interest.

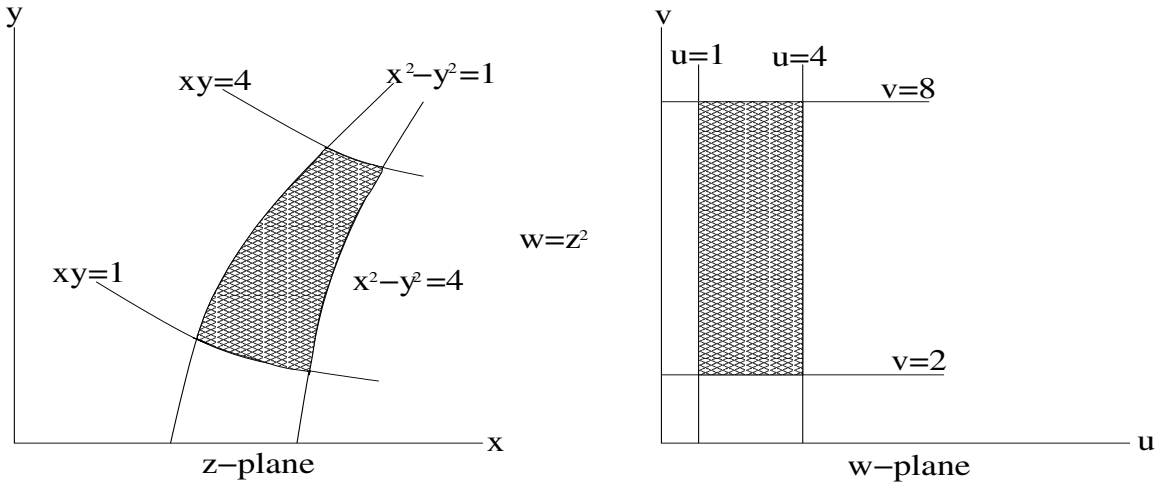

Figure 1: An example of a conformal mapping between the z-plane, $z = x + iy$, and the w-plane, $w(z) = u(x,y) + iv(x,y)$, according to mapping function $w = z^2$. In this example, the shaded region in the z-plane maps to the shaded region in the w-plane. Coordinates (u,v) are given by $(x^2 - y^2, 2xy)$. Lines in the w-plane: $u = 1$, $u = 4$, $v = 2$, and $v = 8$, map to the following lines in the z-plane: $x^2 - y^2 = 1$, $x^2 - y^2 = 4$, $xy = 1$. Note also that orthogonality of line intersections in the w-plane are preserved in the z-plane. jeff1-map1 [NR]

A conformal map is distinguishable from other mappings between complex planes by characteristic properties. Most important to this discussion is the following property:

Conservation of Angle: A conformal mapping of two continuous arcs that locally form an angle α_0 in the z-plane will generate two continuous arcs seperated by the same local angle α_0 in the w-plane.

Figure 1 illustrates the property that grid lines orthogonal in the w-plane are orthogonal in the z-plane under a conformal map. By extension, non-Cartesian orthogonal coordinate systems

can be created in the z-plane (or conversely in the w-plane) by a conformal mapping of a rectangular coordinate system in the w-plane (z-plane).

The first major developments in the theory of conformal mapping originated with the mapping theorem of Riemann (1851), who proved the existence of a unique analytic mapping between any two simply-connected, analytic domains:

Riemann Mapping Theorem: Let D be a simply-connected region. Then there exists a bijective conformal map $f : D \rightarrow U$,where U is the open unit disk. By extension, if G is a another simply-connected domain, there exists a mapping $g : G \rightarrow U$. Hence, there exists a composite mapping operation, $f \cdot g^{-1} : D \rightarrow G$, between two arbitrary simply-connected domains.

Figure 2 illustrates the Riemann mapping theorem between three domains pertinent to the current discussion. Figure 3 presents an example of a conformal mapping between a square and unit circule (the mapping g in Figure 2).

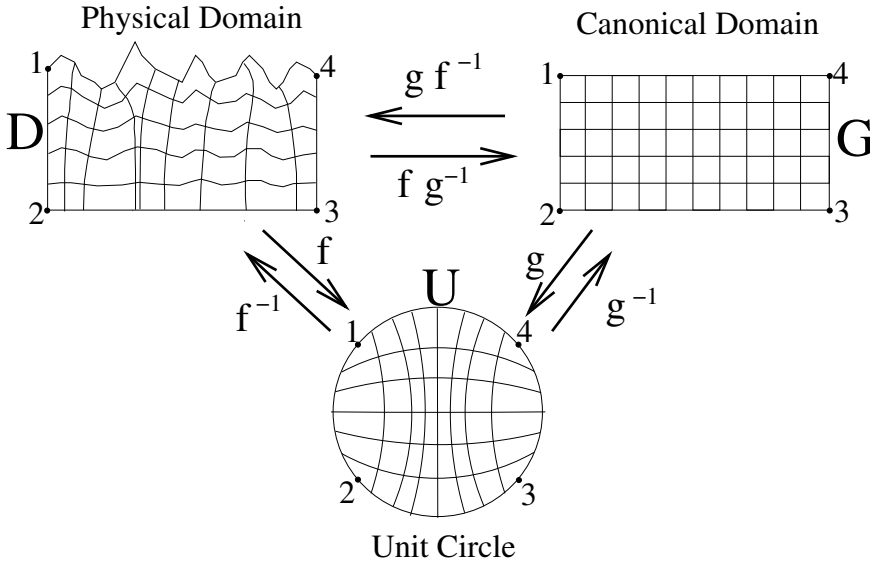

Figure 2: Illustration of the Riemann Mapping Theorem between a physical domain with an undulating upper surface, the unit circle, and a rectangular canonical domain. In this example, a forward mapping function, f, exists between the physical domain and the unit circle and, because the mapping is one-to-one, an inverse mapping f^{-1} also exists. Forward and inverse mapping functions (g and g^{-1}) also exist between the rectilinear domain and the unit circle. Hence, the composition of functions $f \cdot g^{-1}$ denotes a mapping between the physical and canonical domains, while the inverse mapping is given by $g \cdot f^{-1}$. The mapping locations of points labeled 1 through 4 are specified to ensure that the sides in the physical domain correspond to the sides in the canonical domain. jeff1-Riemap [NR]

We will use the Riemann mapping theorem to transform the topographic domain to a rectangular computational mesh. Assisting us is an extensive catalog of conformal maps between

common geometrical domains. Pertinent to the current discussion are the conformal maps between the unit circle (UC) and the upper half plane (UHP), $f : UC \rightarrow UHP$ and its inverse $f^{-1} : UC \leftarrow UHP$,

$$\begin{aligned} f: &\quad z \rightarrow \tfrac{z-i}{z+i}, \\ f^{-1}: &\quad i\tfrac{1+z}{1-z} \leftarrow z, \end{aligned} \tag{1}$$

and the mapping between the UHP and a rectangle with sides of arbitrary length, $g : UHP \rightarrow Rect$, and its inverse $g^{-1} : UHP \leftarrow Rect$,

$$\begin{aligned} g: &\quad w(k) = \int_0^z \frac{\mathrm{d}\zeta}{\sqrt{1-\zeta^2}\sqrt{1-k^2\zeta^2}} \\ g^{-1}: &\quad sn(w;k), \end{aligned} \tag{2}$$

where g is an elliptic integral of the first kind, k is a function of the ratio of the length of the two sides, and $sn(w;k)$ is a Jacobian elliptic function (Nehari, 1975). Appendix A discusses a method for computing conformal map transforms between arbitrary polygons and the UHP.

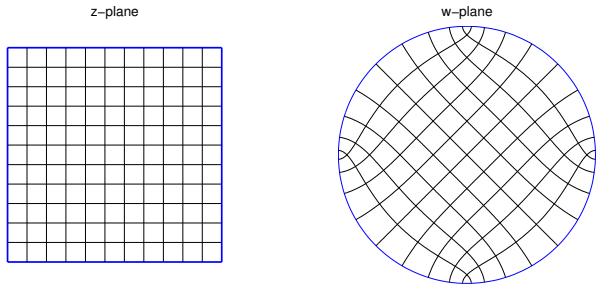

Figure 3: Conformal mapping between a square coordinate system and the unit circle. jeff1-confexamp [NR]

Table 1 outlines a work flow to generate a topographic coordinate system through conformal mapping. The first step is to define the enclosure of the physical domain where the topographic surface defines the upper boundary. We create the lower boundary by mirroring the topography at twice the maximum extrapolation depth. The side boundaries are defined by straight lines that join the top and bottom segments. We denote the border points z^{bnd}_{topo}, where subscript $topo$ and superscript bnd refer to topography and boundary points, respectively. The four corner points of the physical domain are also specified. The next two steps involve calculating the forward and inverse mapping functions, f and f^{-1}, between the topographic surface and the unit circle. The fourth step is to generate a rectilinear boundary and to define its four corner points. We denote this boundary z^{bnd}_{rect}, where subscript $rect$ refers to rectangle. The next two steps involve calculating forward and inverse mappings functions, g and g^{-1}, between the boundary of the rectangle and the unit circle.

To discern where in the canonical domain to form the coordinate system grid, we need to find the mapping of the topography boundary points on the rectangular domain boundary. This is accomplished by calculating the image of the boundary points under composite mapping operations, $z^{bnd}_{im} = g^{-1} \cdot f(z^{bnd}_{topo})$. A rectangular grid is then set up at the image points to create computational grid, z^{cs}_{rect}, where superscripts cs denote coordinate system.

Table 1. Work flow to calculate topographic coordinates with conformal mapping.

Step	Description	Notation
1	Define physical domain boundary and 4 corner points	z_{topo}^{bnd}
2	Calculate mapping $f : Topo \rightarrow UHP \rightarrow UC$	$w_{topo}^{bnd} = f(z_{topo}^{bnd})$
3	Calculate mapping $f^{-1} : UC \rightarrow UHP \rightarrow Topo$	$z_{topo}^{bnd} = f^{-1}(w_{topo}^{bnd})$
4	Define canonical domain border and 4 corner points	z_{rect}^{bnd}
5	Calculate mapping $g : Rect \rightarrow UHP \rightarrow UC$	$w_{rect}^{bnd} = g(z_{rect}^{bnd})$
6	Calculate mapping $g^{-1} : UC \rightarrow UHP \rightarrow Rect$	$z_{rect}^{bnd} = g^{-1}(w_{rect}^{bnd})$
7	Find image of topography in the rectangle	$z_{im}^{bnd} = g^{-1}(f(z_{topo}^{bnd}))$
8	Construct rectilinear grid using $z_{im}^{bnd}(z_{topo}^{bnd})$	z_{rect}^{cs}
9	Map grid z_{rect}^{cs} to physical domain	$z_{topo}^{cs} = f^{-1}(g(z_{rect}^{cs}))$

The final step is to map the rectilinear coordinate system, z_{rect}^{cs}, from the canonical domain back to the topographic coordinates under composite mapping operation, $z_{topo}^{cs} = f^{-1} \cdot g(z_{rect}^{cs})$. Point set z_{topo}^{cs} defines a coordinate system appropriate for performing wavefield continuation directly from topography at the acquisition locations. The next section details how this point set is used to generate the appropriate extrapolation equations.

RIEMANNIAN WAVEFIELD EXTRAPOLATION

Performing wavefield extrapolation on topographic computational meshes computed through conformal mapping requires parameterizing the acoustic wave-equation by a set of variables that describe the coordinate system. In 2-D, we denote these variables the extrapolation direction, τ, (analogous to depth in Cartesian wavefield extrapolation), and the direction orthogonal, γ (analogous to horizontal offset in Cartesian wavefield extrapolation). Variables τ and γ are related to the topographic coordinate system point set through $(\tau,\gamma) = (\Re(z_{topo}^{cs}), \Im(z_{topo}^{cs}))$. Figure 4 presents a sketch of the topographic coordinate system geometry.

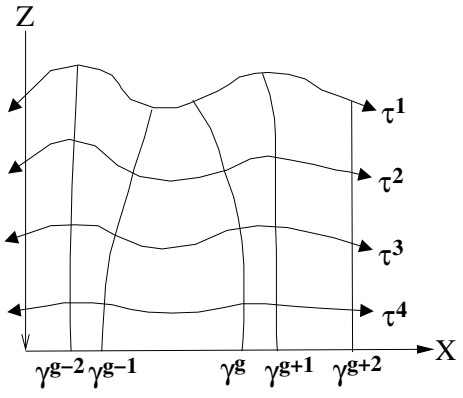

Figure 4: Cartoon illustrating the topography coordinate system. Variable $\tau = \tau(x,z)$ is the extrapolation direction and parameter τ^t may be considered a topographic "front". Variable $\gamma = \gamma(x,z)$ is the coordinate across the extrapolation step at a constant τ step, and parameter γ^g may be considered a topographic "ray". jeff1-topocoord [NR]

The 2-D acoustic wave-equation for wavefield, $\mathcal{U}$, at frequency, ω, governing propagation in topographic coordinates is (Sava and Fomel, 2004),

$$\frac{1}{\alpha J}\left[\frac{\partial}{\partial\tau}\left(\frac{J}{\alpha}\frac{\partial\mathcal{U}}{\partial\tau}\right)+\frac{\partial}{\partial\gamma}\left(\frac{\alpha}{J}\frac{\partial\mathcal{U}}{\partial\gamma}\right)\right]=-\omega^2 s^2\mathcal{U}, \tag{3}$$

where s is the slowness of the medium, α a distance scaling factor in the extrapolation direction τ, and J a Jacobian of transformation of coordinate γ (analogous to a geometrical ray spreading factor). Parameters α and J are defined by,

$$\begin{aligned} \alpha = & \left[\tfrac{\partial x}{\partial \tau}\tfrac{\partial x}{\partial \tau} + \tfrac{\partial z}{\partial \tau}\tfrac{\partial z}{\partial \tau}\right]^{\frac{1}{2}}, \\ J = & \left[\tfrac{\partial x}{\partial \gamma}\tfrac{\partial x}{\partial \gamma} + \tfrac{\partial z}{\partial \gamma}\tfrac{\partial z}{\partial \gamma}\right]^{\frac{1}{2}}, \end{aligned} \tag{4}$$

where x and z are the coordinates of the underlying Cartesian basis. Note that parameters α and J are solely components of the coordinate system and are independent of the extrapolated wavefield values.

Analogous to wavefield continuation on a Cartesian mesh, a dispersion relation must be specified that forms the basis for all derived extrapolation operators in a topographic coordinate system. The relation being sought is the wavenumber along the extrapolation direction, k_τ. Following Sava and Fomel (2004), the partial derivative operators in (3) are expanded out to generate a second-order partial differential equation with non-zero cross derivatives. Fourier-domain wavenumbers are then substituted for the partial differential operators acting on wavefield, $\mathcal{U}$, and the quadratic formula is applied to yield the expression for k_τ,

$$k_\tau = \frac{\mathrm{i}\alpha}{2J}\frac{\partial}{\partial \tau}\left(\frac{J}{\alpha}\right) \pm \left[\omega^2 s^2 \alpha^2 - \left[\frac{\alpha}{2J}\frac{\partial}{\partial \tau}\left(\frac{J}{\alpha}\right)\right]^2 + \frac{\mathrm{i}\alpha}{J}\frac{\partial}{\partial \gamma}\left(\frac{\alpha}{J}\right)k_\gamma - \frac{\alpha^2}{J^2}k_\gamma^2\right]^{\frac{1}{2}}. \tag{5}$$

One relatively straightforward way to apply wavenumber k_τ in an extrapolation scheme is to develop the topographic coordinate system equivalent to a phase-screen extrapolation operator (Sava, 2004). In the following example, we treat solely the kinematic, one-way propagation of recorded wavefields. This asymptotic approximation leads us to drop the first order partial differential terms in (5),

$$k_\tau = \pm\sqrt{a^2\omega^2 - b^2 k_\gamma^2}, \tag{6}$$

where $a = s\alpha$ and $b = \alpha/J$. The expansion of k_τ about reference parameters a_0 and b_0 is,

$$k_\tau \approx k_{\tau 0} + \left.\frac{\partial k_\tau}{\partial a}\right|_{a_0,b_0}(a-a_0) + \left.\frac{\partial k_\tau}{\partial b}\right|_{a_0,b_0}(b-b_0), \tag{7}$$

where subscript 0 denotes reference. Partial derivatives with respect to parameters a and b are,

$$\begin{aligned} \left.\frac{\partial k_\tau}{\partial a}\right|_{a_0,b_0} = & \quad \omega\frac{1}{\sqrt{1-\left(\frac{b_0 k_\gamma}{\omega a_0}\right)^2}} \approx \omega\left[1 + \frac{c_1\left(\frac{b_0 k_\gamma}{\omega a_0}\right)^2}{1-3c_2\left(\frac{b_0 k_\gamma}{\omega a_0}\right)^2}\right], \\ \left.\frac{\partial k_\tau}{\partial b}\right|_{a_0,b_0} = & \quad -\omega\frac{b_0}{a_0}\left(\frac{k_\gamma}{\omega}\right)^2\frac{1}{\sqrt{1-\left(\frac{b_0 k_\gamma}{\omega a_0}\right)^2}} \approx -\omega\frac{b_0}{a_0}\left(\frac{k_\gamma}{\omega}\right)^2, \end{aligned} \tag{8}$$

where the square root function in the denominator has been expanded using a Padé approximation. The choice of numerical constants $c_1 = \frac{1}{2}$ and $c_2 = 0$ yields a 15° finite-difference

term. Thus, the phase-screen approximation for extrapolation wavenumber, k_τ, is,

$$k_\tau \approx k_{\tau 0} + \omega(a-a_0) + \omega \frac{\left[c_1 \left(\frac{a_0}{b_0}\right)^2 (a-a_0) - \frac{b_0}{a_0}(b-b_0)\right]\left(\frac{k_\gamma}{\omega}\right)^2}{1 - 3c_2\left(\frac{b_0}{a_0}\right)^2\left(\frac{k_\gamma}{\omega}\right)^2}. \tag{9}$$

This expression can be generalized to include multiple reference media through a phase-shift plus interpolation (PSPI) approach (Gazdag and Sguazzero, 1984) over the two parameters; however, this extension is not treated here. The approximation for wavenumber, k_τ, given in (9) is used in a conventional wavefield extrapolation scheme that extends the recorded wavefield away from the acquisition surface to the required subsurface locations. This involves solving a one-way wave-equation which, in discrete extrapolation steps of $\Delta\tau$, requires a recursive computation of the following:

$$\mathcal{U}(\tau+\Delta\tau,\gamma,\omega) = \mathcal{U}(\tau,\gamma,\omega)\, \mathrm{e}^{\mathrm{i}k_\tau \Delta\tau}. \tag{10}$$

Our prestack migration example is computed using a shot profile migration code. This involves extrapolating the source and receiver wavefields, $\mathcal{S}$ and $\mathcal{R}$, independently using,

$$\begin{aligned} \mathcal{S}_{\tau+\Delta\tau} &= \mathcal{S}_\tau \mathrm{e}^{-\mathrm{i}k_\tau \Delta\tau}, \\ \mathcal{R}_{\tau+\Delta\tau} &= \mathcal{R}_\tau \mathrm{e}^{\mathrm{i}k_\tau \Delta\tau}, \end{aligned} \tag{11}$$

and applying an imaging condition at each extrapolation level to generate image, $\mathcal{I}(\tau,\gamma)$,

$$\mathcal{I}(\tau,\gamma) = \sum_i \sum_w \mathcal{S}(\tau,\gamma,\omega;\mathbf{s_i})\overline{\mathcal{R}(\tau,\gamma,\omega;\mathbf{s_i})}, \tag{12}$$

where the line over the receiver wavefield indicates complex conjugate. Image $\mathcal{I}(\tau,\gamma)$ is then mapped to a Cartesian coordinate system using sinc-based interpolation operators in the neighborhood of each mapped point to generate the final image, $\mathcal{I}(x,z)$.

NUMERICAL EXAMPLES

We test the combined conformal mapping and Riemannian wavefield extrapolation approach on a synthetic dataset computed on a rugged topographic surface. The geological model is a merger of common geologic features from the Canadian Foothills in northeastern British Columbia, Canada. The velocity model, shown in Figure 5, consists of steep thrust fault planes and complex folds typical of a mountainous thrust region. The topographic boundary of interest is demarcated by the velocity model discontinuity nearest to the surface. The total relief of the Earth's surface in this model is approximately 1600 m. Also note that the complex near-surface velocity structure should present a significant imaging challenge (Gray and Marfurt, 1995).

Figure 6 shows the result of using conformal mapping to construct a coordinate system that incorporates the topography shown in Figure 5. One important observation is that topography

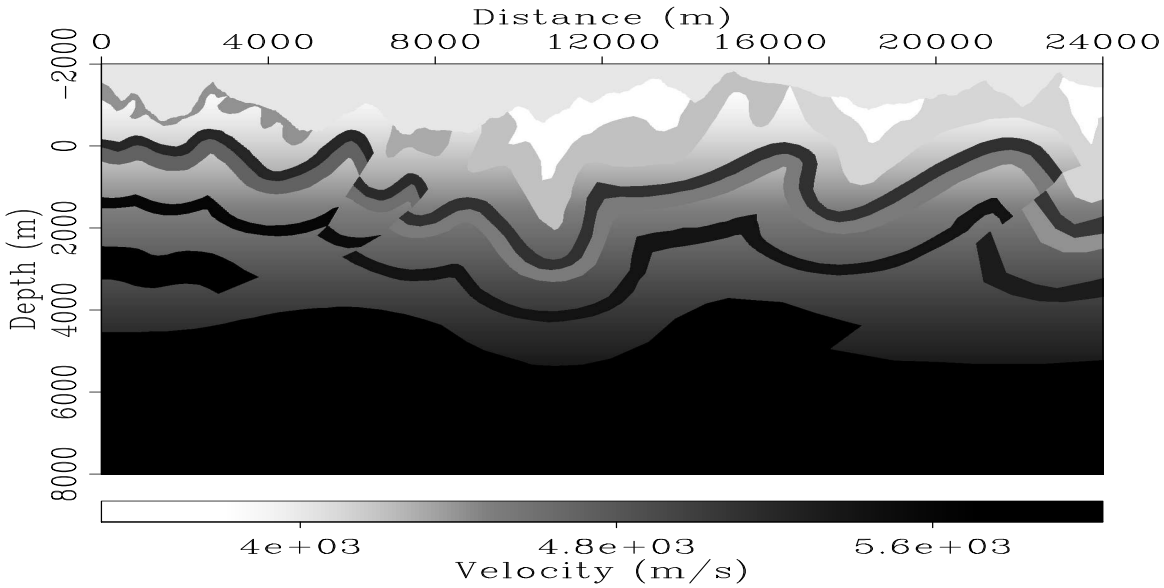

Figure 5: Foothills velocity model constructed from composite 2-D geologic model from northeastern British Columbia, Canada. Total elevation relief is approximately 1600 m. The topographic boundary of interest is demarcated by the velocity model discontinuity nearest to the surface. jeff1-Foothills.vel [ER]

causes focusing of the coordinate system. In particular, the coordinate system compresses under local topographic maxima, and expands beneath local topographic minima. This suggests that Jacobian spreading factor, J, in (3) will be strongly dependent on the local radius of curvature of the topographic surface. However, as the topographic fronts move farther from the surface, the topographic influenced diminishes and the fronts move toward becoming a flat datum. (Hence, this approach could be used for wavefield datuming.)

A prestack wave-equation imaging test was conducted using a synthetic data set generated by an acoustic, 2-D, finite-difference code through the model shown in Figure 5. The data set is comprised of 278 shot gathers with a split-spread geophone geometry where absolute offsets range between 15 m and 3600 m. Geophone and source spacing are 15 m and 90 m, respectively. Data were generated on a regular Cartesian mesh. Thus, we interpolated the data to fit on a grid uniform along the topographic surface. Data fidelity may have been lowered by this processing step; however, we emphasize that this step is normally of modest importance since field data likely are nearly uniformly-spaced on the topographic surface.

A sample shot record at horizontal location 14040 m is shown in Figure 7. Note that the relief causes non-linear moveout of the direct arrival, and a substantial amount of topographic scattering as illustrated by the horizontal banding across the section. No preprocessing of the sections was done to remove these two potential noise sources, and the resulting image is contaminated accordingly.

A preliminary prestack migration image is presented in Figure 8. The majority of reflectors are well positioned; however, diffractions and discontinuous reflectors exist at locations

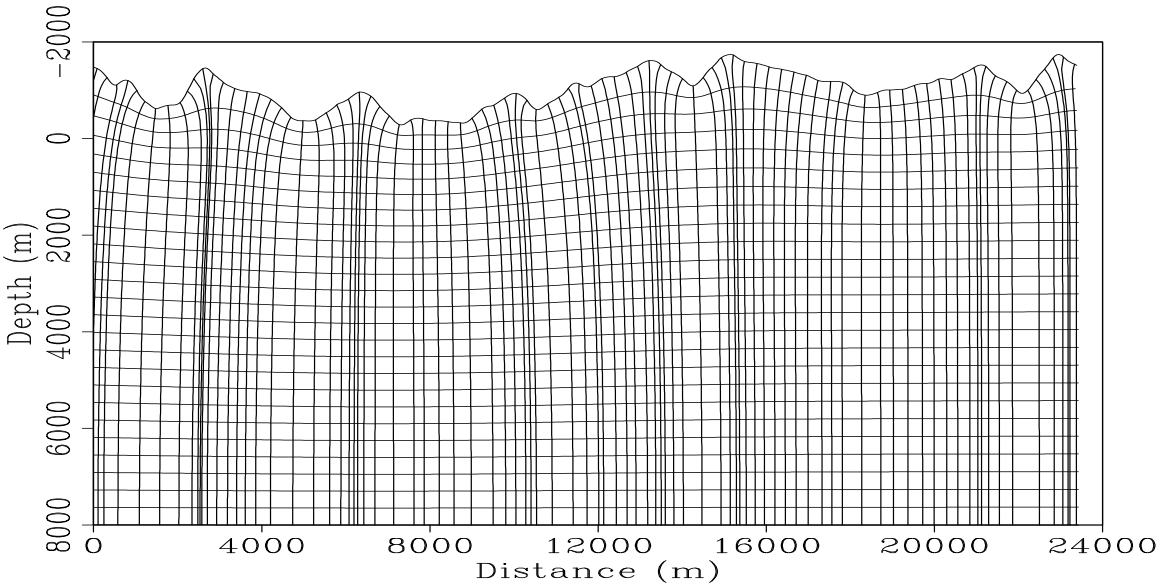

Figure 6: Topographic coordinate system constructed using conformal mapping. Note the compression of the rays under topographic maxima, and their extension under topographic minima. The influence of topography on the coordinate system diminishes farther from the surface. jeff1-Foothills.coords [CR]

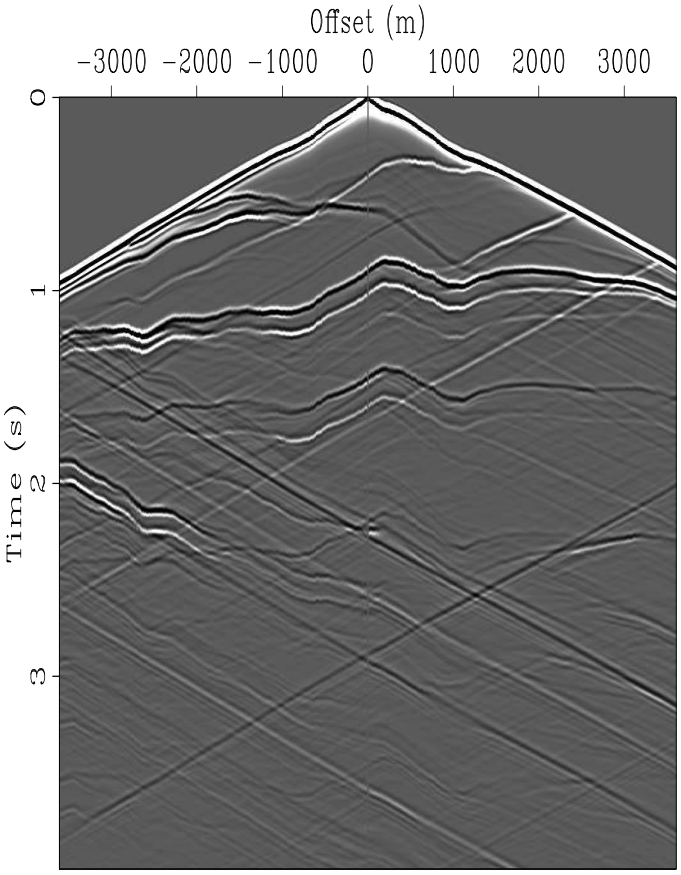

Figure 7: Shot record from source station 14040 m that shows the influence of topography. Note the nonlinear moveout of the direct arrivals, and the significant amount of topographic scattering typified by horizontal streaking across the section. jeff1-singleshot [ER]

directly beneath topographic minima and maxima. Although these anomalies may be caused by the data regularization procedure, they more likely arise from limitations imposed by the phase-screen approximation.

Also present are vertical streaks of higher (lower) amplitude directly under local topographic minima (maxima). We attribute these anomalous amplitudes to a combination of: i) the simplicity of the weighing function used in the interpolation of the image between the topographic and Cartesian coordinate systems; and ii) our non-consideration of the dynamic terms in (6). Geological structure poorly imaged or absent include sections of the steeply-dipping fold belt, which is probably due to limitations imposed by both the limited angular bandwidth of the phase-screen approximation, and our use of only one reference medium.

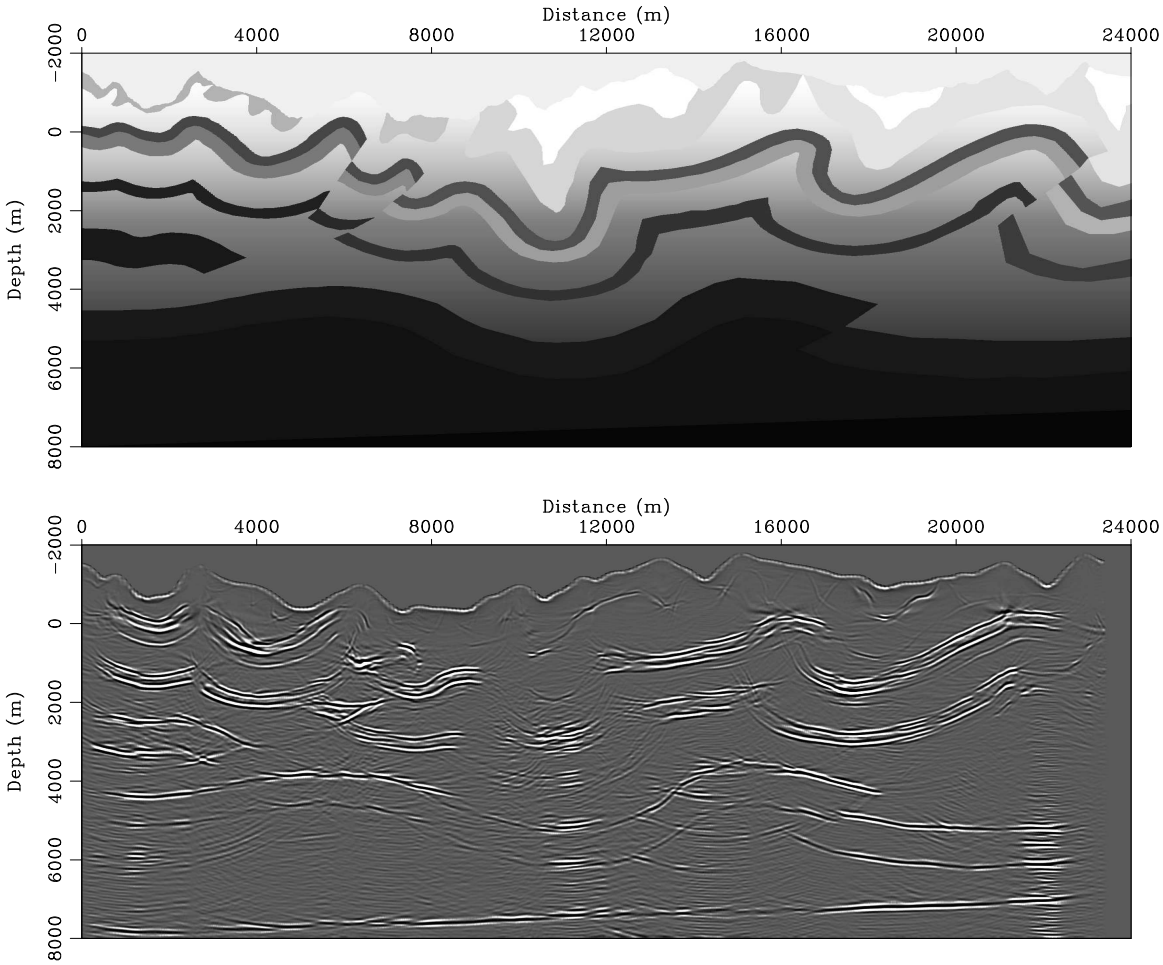

Figure 8: Top: Foothills thrust model velocity model. Bottom: The preliminary prestack migration image using Riemannian wavefield extrapolation on a coordinate system generated through conformal mapping. jeff1-prestackimage [CR]

DISCUSSION AND FUTURE WORK

The issues below are important for improving the quality of wave-equation migration directly from topography images. In some cases, we discuss ideas not yet implemented, while in others we speculate on directions of future research.

Muting direct arrivals: We did not mute out the direct arrivals from the shot gathers, which probably introduced artifacts. In principle, a first-arrival mute is fairly easy to implement; however, their non-linear moveout requires introducing more complicated muting functions. In the future, we will eliminate this source of image contamination.

Using improved mapping weighting functions: We speculate that amplitudes could become more uniform along the reflectors through the use of a better weighting function. The image is currently interpolated to the Cartesian domain using sinc-function operators, where the image points are weighted by the mapping fold. A better weighting function should include the Jacobian of the transformation between the two coordinate systems.

Including dynamic propagation terms: We have incorporated only the second-order partial differential terms in the phase-screen approximation for extrapolation direction wavenumber, k_τ. Including the remaining two dynamic terms should lead to reflectors of more uniform intensity, since these terms contribute to wavefield amplitudes.

Incorporating multiple reference media: The above image was generated using one reference medium (i.e., we performed Taylor expansions about a_0 and b_0). However, in practice many reference media (e.g., velocities) are often used to generate images through the PSPI approach. Noting that the variability of coordinate spacing is significant (and functions a and b thereby), we surmise that the incorporation of multiple reference media is likely necessary to eliminate existing kinematic errors and to improve diffraction focusing.

Implementing a seperate wavefield datuming step: By extension, we have shown that this procedure works as a datuming procedure. For example, a coordinate system generated by conformal mapping could be used in an upward continuation scheme to establish the wavefield at a uniform level above topography. Standard Cartesian migration technology could then be applied directly to migrate the datumed wavefield.

CONCLUSIONS

Performing wave-equation migration directly from topographic surfaces is achievable with a minimum of preprocessing in topographic coordinate systems. We show that conformal mapping generates the required topographic coordinate systems, and that the conformal map transform determines the appropriate wavefield extrapolation equations. We also conclude that multiple reference media are likely needed to image under complicated topography, which is consistent with wavefield extrapolation practice in a Cartesian coordinate system.

By extension, we show that upward datuming on a coordinate system generated through conformal mapping transformation could work as a pre-imaging processing step. Moreover, upward datuming could be more effective than downward migration direct from topography, since a constant velocity function would likely improve the range over which the phase-screen approximation is accurate. Standard Cartesian-based migration technology could then be used to downward continue the upward datumed wavefields.

ACKNOWLEDGMENTS

We acknowledge BP for providing the data set used in the prestack migration example, and would like to thank Bee Bednar and Biondo Biondi for helpful discussions.

REFERENCES

Berryhill, J., 1979, Wave-equation datuming: Geophysics, **44**, 1329–1344.

Bevc, D., 1997, Floodint the topography: Wave-equation datuming of land data with rugged acquisition topography: Geophysics, **62**, 1558–1569.

Gazdag, J., and Sguazzero, P., 1984, Migration of seismic data by phase-shift plus interpolation: Geophysics, **69**, 124–131.

Gray, S., and Marfurt, K., 1995, Migration from topography: Improving the near-surface image: J. Can. Soc. Expl. Geophys., **31**, 18–24.

Jiao, J., Trickett, S., and Link, B., 2004, Wave-equation migration of land data: 2004 CSEG Convention, CSEG, CSEG Abstracts.

Kythe, P., 1998, Computational conformal mapping: Birkhäuser, Boston, MA.

Nehari, Z., 1975, Conformal mapping: Dover Publications Inc., New York.

Riemann, B., 1851, Grundlagen für eine allgemeine Theorie der Funktionen einer veränderlichen komplexen grösse (1851) in collected works: Dover Publications Inc, New York.

Sava, P., and Fomel, S., 2004, Seismic imaging using Riemannian wavefield extrapolation: submitted to Geophysics.

Sava, P., 2004, High-order kernels for Riemannian wavefield extrapolation: SEP–**117**.

APPENDIX A

This appendix discusses the conformal mapping between polygons of arbitrary shape and the upper half plane. Assisting us in this transformation is an important conformal map transformation, termed Schwarz-Christoffel mapping, that facilitates solution of a class of BVPs with polygonal boundaries. Figure A-1 illustrates the transformation and also illustrates the basic nomenclature.

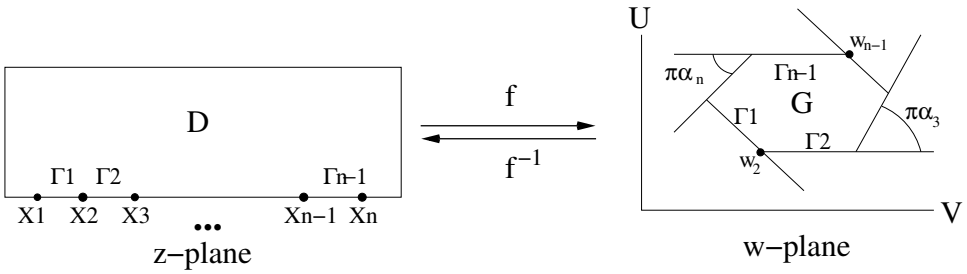

Figure A-1: Schematic of the Schwarz-Christoffel transformation between a polygonal domain in the w-plane and the upper half plane (UHP), $D = z : \Im(z) > 0$, in the z-plane. This transformation maps line segments Γ_i that lie on the $y = 0$ line in the z-plane to the line segments Γ_i that define the polygonal boundary of the w-plane according to mapping rule f. Exterior angles, $\pi\alpha_i$, are used in the transformation formula, and are defined by $|\alpha_i| > 1$ and $\sum_{i=1}^{n} \alpha_n = 2$. Points x_i in the z-plane are mapped to points w_i in the w-plane. jeff1-sctran [NR]

The formula for calculating the transformation is,

$$w = f(z) = A + B \int_{z_0}^{z} \prod_{i=1}^{n} (\zeta - x_i)^{-\alpha_i} \, \mathrm{d}\zeta, \tag{A-1}$$

where A and B are constants that determine the size and position of the polygon Γ, and α_i denotes the exterior angle (see Figure A-1). Constants A and B are computed after defining the mapping of 3 points (i.e., known points z_0). The integration is carried out along any path in the domain D that connects known point z_0 and the point in question z.

The inverse Schwarz-Christoffel transformation is given by,

$$z = f(w) = C_0 + C \int_{w_0}^{w} \prod_{i=1}^{n} (\zeta - w_i)^{-\mu_i} \, \mathrm{d}\zeta, \tag{A-2}$$

where μ_i are the interior angles, and integration is carried out along any path that connects known mapping point w_0 with the point in question w.

In numerical applications of Schwarz-Christoffel mapping, it is necessary to determine numerically the (2n+2) parameters (i.e. all α_i, x_i and A, B) that appear in equations (A-1) and (A-2). In conformal mapping literature, this problem is termed the 'parameter problem'

(Kythe, 1998). The numerical solution to this problem requires selecting 3 points of the x-axis that map to 3 preassigned points in the u-axis (i.e. p_1, p_2 and p_3). This allows for equation (A-1) to be segmented into the Schwarz-Christoffel integrals,

$$\begin{aligned} I_1 = &\quad \int_{p_1}^{p_2}(\zeta-p_1)^{-\alpha_1}(\zeta-p_2)^{-\alpha_2}(\zeta-p_3)^{-\alpha_3}...(\zeta-p_{n-1})^{-\alpha_{n-1}}(\zeta-p_n)^{-\alpha_n}\mathrm{d}\zeta \\ I_2 = &\quad \int_{p_2}^{x_3}(\zeta-p_1)^{-\alpha_1}(\zeta-p_2)^{-\alpha_2}(\zeta-p_3)^{-\alpha_3}...(\zeta-p_{n-1})^{-\alpha_{n-1}}(\zeta-p_n)^{-\alpha_n}\mathrm{d}\zeta \\ \vdots &\qquad\qquad\qquad \vdots \\ I_{n-2} = &\quad \int_{x_{n-2}}^{x_{n-1}}(\zeta-p_1)^{-\alpha_1}(\zeta-p_2)^{-\alpha_2}(\zeta-p_3)^{-\alpha_3}...(\zeta-p_{n-1})^{-\alpha_{n-1}}(\zeta-p_n)^{-\alpha_n}\mathrm{d}\zeta \end{aligned} \tag{A-3}$$

Fortunately, the ratio of any two sides of the mapped polygon is independent of scale factors A and B. This allows the parameter problem to be written as the following series of equations:

$$I_j(x_3,x_4,...,x_{n-1}) = \lambda_j I_1(x_3,x_4,...,x_{n-1}), \quad j=2,3,...,n-2, \tag{A-4}$$

where

$$\lambda_j = \frac{|w_{j+1}-w_j|}{|w_2-w_1|} \quad j=3,4,...,n-2. \tag{A-5}$$

A solution to the Schwarz-Christoffel integrals begins by expanding the series of equations (A-5) in a first order Taylor power series about initial guesses, $x_i^{(0)}$, of the true values, $\tilde{x}_i$. This leads to a system of equations that may be solved using Newton's method:

$$I_j^{(0)} + \sum_{\nu=3}^{n-1} h_\nu^{(1)} \frac{\partial I_j^{(0)}}{\partial x_\nu} = \lambda_j \left[I_1^{(0)} + \sum_{\nu=3}^{n-1} h_\nu^{(1)} \frac{\partial I_1^{(0)}}{\partial x_\nu} \right], \quad j=2,...,n-2, \tag{A-6}$$

where h_ν, the correction factors that are being solved for, are applied to yield the next estimate of the vertex corners,

$$x_\nu^{(0)} = x_\nu^{(0)} + h_\nu^{(1)}. \tag{A-7}$$

This process is repeated using nth iterative updates of $h_\nu^{(n)}$ until the desired tolerance is reached. Finally, the Schwarz-Christoffel integrals are improper because the integrand of each integral becomes unbounded at the two points of integration. Kythe (1998) discusses using the Kantorovich method to regularize these integrals.